Available online at www.sciencedirect.com
SCIENCE DIRECT
International Journal of Heat and Mass Transfer 49 (2006) 4231–4249
International Journal of HEAT and MASS TRANSFER
www.elsevier.com/locate/ijhmt

3-D modeling of the dynamics and heat transfer characteristics of subcooled droplet impact on a surface with film boiling

Yang Ge, L.-S. Fan *

Department of Chemical and Biomolecular Engineering, The Ohio State University, Columbus, OH 43210, United States

Received 3 October 2005; received in revised form 24 February 2006
Available online 27 June 2006

Abstract

The impact of a subcooled water and *n*-heptane droplet on a superheated flat surface is examined in this study based on a three-dimensional model and numerical simulation. The fluid dynamic behavior of the droplet is accounted for by a fixed-grid, finite-volume solution of the incompressible governing equations coupled with the 3-D level-set method. The heat transfer inside each phase and at the solid–vapor/liquid–vapor interface is considered in this model. The vapor flow dynamics and the heat flux across the vapor layer are solved with consideration of the kinetic discontinuity at the liquid–vapor and solid–vapor boundaries in the slip flow regime. The simulated droplet dynamics and the cooling effects of the solid surface are compared with the experimental findings reported in the literatures. The comparisons show a good agreement. Compared to the water droplet, it is found that the impact of the *n*-heptane droplet yields much less surface temperature drop, and the surface temperature drop mainly occurs during the droplet-spreading stage. The effects of the droplet's initial temperature are also analyzed using the present model. It shows that the droplet subcooling degree is related closely to the thickness of the vapor layer and the heat flux at the solid surface.

1. Introduction

The impact of liquid droplets on a superheated surface is of great importance to many industrial applications. Examples of such impact include diesel fuel droplets contacting the cylinder wall, sprinkler cooling in the iron-making or metal casting process, spray coating of the substrate and the liquid jet in gas–solid flow systems [1,2]. In most of these applications, the solid surface temperatures are above the Leidenfrost temperature of the droplet liquid; under this condition the droplet evaporation is in the film-boiling regime [3]. The nature of the collision of the droplet with the superheated surface exhibits great diversity in hydrodynamic and thermodynamic properties, such as droplet splash and rebound, wetting or non-wetting contact, nucleate boiling or film boiling, and Marangoni effect. Further, the droplet shape, the contact area and the cooling effectiveness during the impact not only depend on such hydrodynamic forces as the inertia, pressure, surface tension and the viscosity forces but also on the degrees of the surface superheating and the droplet sub-cooling [4–6]. In the impact with the isothermal surface, the droplet dynamics can be determined by two dimensionless variables [7]:

$$Re = \rho V_0 d_0/\mu, \quad We = \rho V_0^2 d_0/\sigma$$

along with the roughness of the surface and the wettability. V_0, and d_0 are the droplet velocity and diameter before the impact, respectively; ρ, σ, and μ are the density, surface tension and viscosity of the liquid, respectively. As the solid surface temperature increases to a superheated condition, the characteristics of the liquid–solid contact significantly change and the evaporation becomes important in affecting the droplet dynamics. Wachters and Westerling [4] studied the saturated impact of water droplets on a golden surface, in which the initial temperature of the droplet is the saturation temperature of the liquid. They found that as the

* Corresponding author. Tel.: +1 614 292 6591; fax: +1 614 292 3769.
E-mail address: FAN@er6s1.eng.ohio-state.edu (L.-S. Fan).

0017-9310/$ - see front matter © 2006 Elsevier Ltd. All rights reserved.
doi:10.1016/j.ijheatmasstransfer.2006.03.023

Nomenclature

$\widetilde{D}$	stress tensor
d	droplet diameter
g	gravitational acceleration
H	Heaviside function
k	heat conductivity
Kn	Knudsen number
L_c	latent heat
Pr	Prandtl number
p	pressure
q	heat flux
r	radial direction
R	radius of the contact area
Re	Reynolds number
T	temperature
t	time
u	velocity of the vapor flow
$\boldsymbol{V}$	velocity
$\dot{m}$	mass evaporation rate
We	Weber number
z	normal direction to the surface

Greek symbols

α	thermal diffusivity
δ	δ function (or the thickness of the vapor layer and thermal boundary layer)
ϕ	level-set function
ν	kinematics viscosity of vapor flow
κ	curvature of the surface
λ	mean free path of gas molecule
μ	molecular viscosity
ρ	density
σ	surface tension
σ_t	thermal accommodation coefficient
Δ	grid size

Subscripts and superscripts

d	droplet
g	gas phase
l	liquid phase
0	initial
s	solid
sa	saturated
v	vapor phase
Γ	droplet surface

temperature of the surface increases from 170 °C to 400 °C, the liquid–solid contact gradually decreases, yielding a decrease in heat flux through the surface and an increase in droplet evaporation time. When the surface temperature becomes 400 °C, the droplet evaporates in a purely spheroidal, non-wetting state and the Weber number can be used to describe the droplet dynamics. Biance et al. [8] studied the steady state evaporation of a water droplet on a superheated surface and found that, in a non-wetting contact condition, the droplet size cannot exceed the capillary length.

For subcooled impacts, the initial droplet temperature is below the liquid saturation temperature. The subcooled impact represents most of the practical applications, since the temperatures of the liquid droplet evolved from liquid spray are usually equal to that of the ambient condition to which the droplet is exposed. Chandra and Avedisian [6] studied the collision dynamics of a 24 °C *n*-heptane droplet impacting on a metallic surface with the Weber number equal to 43. The transition from the nucleate boiling to the film boiling was identified when the surface temperature rises from the boiling point (170 °C) to above the Leidenforost temperature (200 °C) of *n*-heptane. They found that under the film-boiling limit, the liquid–solid contact is hindered by the vapor layer as evidenced by the disappearance of the bubbles inside the liquid droplet under the nucleate boiling condition. The contact angle of the liquid to the surface was also reported to increase with an increase in the surface temperature, reaching 180° in the film boiling condition. Qiao and Chandra [9] measured the temperature drop of a stainless steel surface during the impact of the subcooled water and *n*-heptane droplets in low gravity. They found that when the surface temperature is above the superheat limit, the temperature drop of the surface is relatively small for the impact of a *n*-heptane droplet (less than 20 °C). For the impact of a water droplet, however, the temperature drop on the surface can reach as high as 150 °C, which implies a high heat flux and the intermitted contact of the liquid and the solid surface. Hatta et al. [10] found that, under low impact velocity or a low *We* number, the dynamics of the water droplet is almost independent of the surface materials when the surface temperature is above the Leidenfrost condition. Nevertheless, the properties of the surface do affect the occurrence of the droplet disintegration at a higher *We*, which was regarded as the evidence for direct liquid–solid contact.

The effects of the initial droplet temperature or the degree of subcooling on the film-boiling impact were studied by Inada et al. [5]. They found that the heat transfer rate on the solid surface during an impact of a 4 mm water droplet increases significantly with a decrease in the initial droplet temperature. The boiling regime is classified to represent different droplet dynamic and heat transfer modes at

various droplet and surface temperatures. Inada et al. [11] also measured the thickness of the vapor film between the impinging droplet and the surface at varied degrees of subcooling. Chen and Hsu [12] measured the transient local heat flux at the surface of a pre-superheated plate which underwent the impingement of subcooled water droplets. A fast response micro-thermocouple was designed to capture the instantaneous changes of the solid surface temperature. Although the droplet dynamics of the impact process were not presented, they concluded that both the surface temperature and the degree of the droplet subcooled are crucial to the intermittent contact mode at the solid surface. For the droplet with a subcooling of 80 °C, it was found that the heat flux at the solid surface could reach $\sim 10^7$ W/m^2 at the initial stage of the droplet impact which, according to the author, implies liquid–surface direct contact. As the surface temperature rises from 150 °C to 400 °C, the time duration of this higher heat flux becomes significantly shorter (from 28 ms to 7 ms). At the film boiling regime, with the surface temperature superheated to 400 °C, the subcooled droplet trends to disintegrate during the impact at $We = 55$.

Several numerical models have been developed to describe the hydrodynamics of the droplet impact on a surface. Harlow and Shannon [13] first applied the MAC (marker-and-cell) method to simulate the droplet impact without considering the viscosity and surface tension forces in the momentum conservation equation. Fukai et al. [14] simulated the droplet colliding with a surface using the adaptive-grid finite element method and the wettability on the contact line was also considered. Pasandideh-Ford et al. [15] used a modified SOLA-VOF method to solve the momentum and heat transfer equations for droplet deposition on a steel surface. Bussmann et al. [7,16] developed a 3-D model to simulate the droplet collision onto an inclined surface and its splash on the surface, utilizing a volume tracking methodology. Mehdi-Nejad et al. [17], also used the VOF method to simulate the bubble entrapment behavior in the droplet when it impacts a solid surface. Francois and Shyy [18] simulated the droplet impact dynamics using the immerse boundary (IB) method and the effects of *We* and *Re* were studied.

Efforts have also been made on probing the phenomenon of the droplet impact onto a superheated surface with evaporation. Karl et al. [19] simulated small droplet (100–200 μm) impact onto a wall in the Leidenfrost regime using a VOF (volume of fluid) method. A free-slip boundary condition and a 180° contact angle were applied on the solid surface. Fujimoto and Hatta [20] simulated the dynamics of droplet impingement by using a two-dimensional MAC-type solution method. They applied the no-slip boundary condition on the solid–liquid surface in the droplet spreading stage, which was followed by the free-slip boundary condition in the recoiling stage. Harvie and Fletcher [21,22] developed an axisymmetric, 2-D volume of fluid algorithm to simulate the volatile liquid droplet impacting on a hot solid surface. The vapor flow between the droplet and solid surface was described by a one-dimensional, creeping flow model, which neglects the inertial force of the flow. This model can predict the droplet dynamics accurately at the Weber number below 30. When the Weber number is above 30 (e.g. $We = 74$), their model could predict the spreading process of the droplet, but not predict the recoiling and rebound processes of the droplet. The deficiency of their prediction might be due to the two-dimensional nature of the model. More recently, Chizhov and Takayama [23] studied impact of a liquid nitrogen droplet on a hot surface with a high velocity where the consideration of the compressibility of the liquid becomes important.

Little is reported on the 3-D simulation of the droplet impact on the solid surface at high temperatures. Ge and Fan [24] developed a three-dimensional, finite-volume numerical model to simulate saturated droplet impact on a flat surface in the Leidenfrost regime. Their model was coupled with the level-set method to track the droplet surface and a two-dimensional vapor flow model was developed to account for the vapor flow behavior between the droplet and the surface without neglecting the inertial force of the vapor. The energy equations were solved to determine the evaporation rate and temperature distribution in the solid phase. The ALE technique was employed to solve the fluid governing equations. The object of this study is to develop a three-dimensional model to describe the collision mechanics of a subcooled droplet with a superheated surface. The droplet deformation is tracked by the use of the level-set method, and a vapor layer model is utilized to account for the vapor pressure force due to the evaporation. The transient heat transfer inside the droplet and solid surface is considered. Since the thickness of the vapor layer may be comparable with the mean free path of the gas molecules in the subcooled impact, the boundary condition for the continuum system needs to be modified to allow the kinetic slip treatment to be applied to the liquid–vapor and vapor–solid interfaces. The droplet dynamics and the heat transfer at the surface are predicted and compared with the experimental data reported in the literature. The effects of the droplet subcooling degree on impact are analyzed.

2. Mathematical models and numerical methods

2.1. Hydrodynamic model

The flow field of the impacting droplet and its surrounding gas is simulated using a finite-volume solution of the governing equations in a three-dimensional Cartesian coordinate system. The fluid is assumed to be incompressible and the equations of conservation of mass and momentum are

$$\nabla \cdot \vec{V} = 0 \tag{1}$$

$$\rho\left(\frac{\partial \vec{V}}{\partial t} + \nabla \cdot \vec{V}\vec{V}\right) = -\nabla p + \rho\vec{g} + \nabla \cdot (2\mu\tilde{D}) + \sigma\kappa(\phi)\delta(\phi)\nabla\phi \tag{2}$$

where $\vec{V}$ is the fluid velocity; p represents the pressure; ρ is the pressure; μ is the fluid viscosity and $\widetilde{D}$ is the viscous stress tensor. The surface tension force given in the last term of Eq. (2) is included in this model as a body force and is expressed using the continuum surface model (CSM) [25]. This force acts only on the computational cells in the vicinity of the free surface. σ is the surface tension coefficient; $\delta(\phi)$ is the one-dimensional delta function; $\kappa(\phi)$ is the curvature of the free surface; and ϕ is the level-set function which will be described below. It should be noted that these equations are applied to the entire computational domain, which includes both the liquid phase and the gas phase. This is accomplished by assigning proper fluid properties ρ and μ to either the gas or the liquid phase based on their corresponding locations to the interface. To solve the governing equations, an explicit cell-centered ICE (implicit continuous-fluid Eulerian) numerical technique is employed based on the CFDLIB code [26] in which the ALE (Arbitrary Lagrangian Eulerian) technique is applied to support the arbitrary mesh motion with fluid flows.

The level-set method [27] is employed in this model to simulate the movement and deformation of the free surface of the droplet during impact. In this method, the zero level set of a smooth scalar function, the level-set function $\phi(\vec{x},t)$, is defined to represent the droplet surface. Since the interface is advected by the flow and the fluid is assumed incompressible, the motion of the interface can be traced using:

$$\frac{\partial\phi}{\partial t}+\vec{V}\cdot\nabla\phi=0 \tag{3}$$

In the discretization of this equation, the level-set function $\phi_{i,j,k}$ is a signed scale whose absolute value is equal to the distance from the computational cell (i,j,k) to the interface. ϕ is greater than 0 when a cell is in gas phase and ϕ is less than 0 when a cell is in liquid phase. The droplet surface is represented by ϕ with a value of zero. To solve Eq. (3), a high order ENO upwind scheme [28] is used to calculate the convective term $\vec{V}\cdot\nabla\phi$, and the second-order TVD Runge–Kutta method is employed to advance the time step [29]. The calculation is followed by an iterative re-distancing procedure for setting the level-set function to be equal to the distance function and for maintaining the mass conservation. Details of this procedure are presented in Sussman et al. [28].

As the interface can be identified by the level-set function, the averaged fluid density ρ and viscosity μ used in Eq. (2) can then be defined as

$$\rho=\rho_{\mathrm{l}}+H(\phi)(\rho_{\mathrm{g}}-\rho_{\mathrm{l}}) \tag{4}$$

$$\mu=\mu_{\mathrm{l}}+H(\phi)(\mu_{\mathrm{g}}-\mu_{\mathrm{l}}) \tag{5}$$

where ρ_{l} and ρ_{g} are the density of the liquid and gas, respectively; and μ_{l} and μ_{g} are the viscosity of the liquid and gas, respectively. $H(x)$ is a smoothed Heaviside function [29].

During the subcooling droplet impact, the droplet temperature undergoes significant changes due to heat transfer from the high temperature surface. As the liquid properties such as density $\rho_{\mathrm{l}}(T)$, viscosity $\mu_{\mathrm{l}}(T)$ and surface tension $\sigma(T)$ vary with local temperature T, the local liquid properties can be quantified once the local temperature is known. The droplet temperature is simulated by the following heat transfer model and vapor layer model. Since the liquid temperature changes from its initial temperature (usually room temperature) to the saturated temperature of the liquid during the impact, a linear variation of liquid properties with temperature is assumed, which is

$$\gamma(T)=\gamma_0+\frac{T-T_0}{T_{\mathrm{sa}}-T_0}(\gamma_{\mathrm{sa}}-\gamma_0)\quad \gamma=\rho_{\mathrm{l}},\mu_{\mathrm{l}},\sigma \tag{6}$$

where T_0 and T_{sa} are the initial temperature and saturated temperature of the liquid respectively; γ_0 and γ_{sa} are the liquid properties at T_0 and T_{sa}, respectively.

Since the impacts of the droplets simulated in this study are all under the condition that the surface temperature is higher than the Leidenfrost temperature of the liquid, it is assumed that the direct contact of the droplet and the surface is prevented by a micro-scale vapor layer. Therefore, the wetting effect is neglected [20], and the no-slip boundary condition is adopted at the solid surface during the droplet spreading process and the free-slip condition is applied for the recoiling and rebounding periods. The computational domain covers both the fluid (droplet and the surrounding gas) and the solid surface. The relative boundary condition is applied by resetting the velocity at the grid points inside the solid surface at each time step.

2.2. Heat transfer model

For the subcooled impacts, especially for the high subcooling degree case in which the droplet's initial temperature is much lower than the saturated temperature, the heat transfer within the droplet is significant and hence affects the droplet evaporation rate. Neglecting the viscous dissipation, the equation of the conservation of the thermal energy inside the droplet is given by

$$\frac{\partial T}{\partial t}+\vec{V}\cdot\nabla T=\alpha_{\mathrm{l}}\nabla\cdot\nabla T \tag{7}$$

where α_{l} is the thermal diffusivity of liquid. Note that this equation can only be used to solve the temperature distribution inside the droplet when the boundary condition at the interface is properly imposed. In this study, it is assumed that the heat transfer across the droplet interface only occurs at the location where the droplet surface is in contact with the vapor layer or solid surface. At other parts of the free surfaces of the droplet, the adiabatic boundary condition is applied which is given by

$$\vec{n}_{\Gamma}\cdot\nabla_{\mathrm{d}}T=0 \tag{8}$$

where $\vec{n}_{\Gamma}$ is the normal vector of the droplet surface, which can be calculated based on the level-set function:

$$\vec{n}_\Gamma = \frac{\nabla\phi}{|\nabla\phi|} \tag{9}$$

$\nabla_d T$ is the temperature gradient, which is evaluated only on the droplet side. In a three-dimensional simulation, the interface boundary condition is imposed on the computational cells, which are located in a small band near the interface on the liquid side. The thickness of this band is chosen to be equal to 1.5Δ, where Δ is the mesh size. At each time step, the temperature at the grid point inside this band is recalculated by Eq. (8). In this process, the gradients of T are evaluated based only on the grid point in the liquid side.

The heat conduction inside the solid surface is given by

$$\frac{\partial T_s}{\partial t} = \alpha_s \nabla \cdot \nabla T_s \tag{10}$$

where T_s is the solid temperature and α_s is the thermal diffusivity of solid.

Fig. 1 shows the notations and relative relationships of the temperature distribution and heat flux across the vapor layer for given temperatures in the solid, liquid and vapor phases. The main assumption made in the model is that the height of the vapor layer (~μm) is very small compared with the radius of the droplet (~mm) [24]. The radiation heat transfer is negligible since the temperature of the surface is less than 700 °C [21,22]. In the subcooled impact, especially for a droplet of water (which has a larger latent heat), it has been reported that the thickness of the vapor layer can be very small (less than 1 μm) and, in some cases, the transient direct contact of the liquid and the solid surface may occur [12]. When the length scale of the vapor gap is comparable with the free path of the gas molecules, the kinetic slip treatment of the boundary condition needs to be undertaken to modify the continuum system. Consider the Knudsen number defined as the ratio of the mean free path of the vapor to the thickness of the vapor layer:

$$Kn = \frac{\lambda}{\delta} \tag{11}$$

where λ is the mean free path of the molecule, which was estimated to be ~0.01 μm for vapor gas [30]. Therefore the Knudsen number for the vapor flow can be larger than 0.01. Harvie and Fletcher [31] analyzed the kinetics of the molecular behavior at the solid and the evaporative surface for $0.01 < Kn < 0.1$. Based on their simplified kinetic theory, the effective temperature discontinuity at the liquid–vapor surface and the solid–vapor surface can be given by

$$T_{s2} - T_{s1} = C_{T,s}(T_{s1} - T_{d2}) \tag{12}$$

$$T_{d1} - T_{d2} = C_{T,l}(T_{s1} - T_{d1}) \tag{13}$$

where T_{s1}, T_{s2}, T_{d1}, T_{d2} are the interface temperatures of the solid surface and the droplet shown in Fig. 1. C_T is defined by

$$C_T = Kn\left(\frac{9}{4}\gamma - \frac{5}{4}\right)\left(\frac{2-\sigma_t}{\sigma_t}\right) \tag{14}$$

In Eq. (14), σ_t is the thermal accommodation coefficient defined by Harvie and Fletcher [31]. At the liquid–vapor interface, since the vapor layer thickness is much smaller than the flow-scale, such as the droplet diameter, the energy conservation equation for the vapor phase can be simplified to a 1-D equation:

$$k_v \frac{T_{s1} - T_{d1}}{\delta} = q_l + \dot{m}L_c \tag{15}$$

where k_v is the thermal conductivity of the vapor; L_c is the latent heat of the liquid; q_l is the heat flux at the droplet surface at the liquid side, which is given by $q_l = -k_l \nabla_d T$.

The numerical method for solving the heat transfer equation in the liquid and solid phases is a finite-volume, ALE method [26]. The heat diffusion is calculated in a Lagrangian phase followed by a remapping phase to compute the convection. The boundary conditions at the solid surface and droplet–vapor interface are imposed during each time-step.

2.3. Vapor layer model

Since the thickness of the vapor layer (~μm) is several orders of magnitude smaller than the macro-flow scale, (i.e. the diameter of the droplet), a 2D model developed earlier by the authors [24] based on a reduced N–S equation is used to simulate the dynamics of the vapor flow between the droplet and the surface. This model involves the continuum assumption in treating the vapor momentum. This assumption, however, needs to be modified by considering the kinetic slips at the boundary when the Knudsen number of the vapor is larger than 0.01 [30].

In the film-boiling regime, the evaporation of the droplet is so intensive that the vapor layer is formed as soon as the droplet approaches the surface. It is assumed that the gas phase in the vapor layer is composed only by the saturated vapor of the droplet liquid. In the symmetrical coordinates (r,z), assuming that vapor flow is in a steady state, the continuity and momentum equations for incompressible vapor flows can be reduced with the assumption that the thickness of the vapor layer is much smaller than the radius of the droplet:

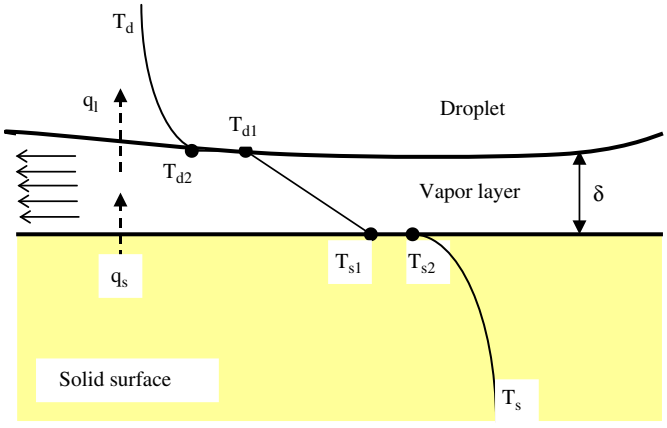

Fig. 1. Temperature distribution and heat flux across the vapor layer.

$$\frac{\partial u_r}{\partial r}+\frac{u_r}{r}+\frac{\partial u_z}{\partial z}=0 \tag{16}$$

$$u_r\frac{\partial u_r}{\partial r}+u_z\frac{\partial u_r}{\partial z}=-\frac{\partial}{\partial r}\left(\frac{P}{\rho}\right)+v\frac{\partial^2 u_r}{\partial z^2} \tag{17}$$

When the Knudsen number of the vapor flow is between 0.01 and 0.1, the flow is in the slip regime. In this regime, the vapor flow can be considered as a continuum at a distance of several mean free paths away from the boundary; however, an effective slip velocity needs to be considered in describing the molecular interaction between the gas phase and the boundary. Based on the simple kinetic analysis of vapor molecules near the interface [31], the boundary conditions of the vapor flow at the solid surface can be given by

$$\begin{aligned} &Z=0,\quad u_r(r,0)=F_s\frac{\partial u_r}{\partial z}(r,0)\\ &u_z(r,0)=0 \end{aligned} \tag{18}$$

and the boundary conditions at the droplet surface are

$$\begin{aligned} &Z=\delta,\quad u_r(r,\delta)-u_{r,l}(r)=F_l\frac{\partial u_r}{\partial z}(r,\delta)\\ &u_z(r,\delta)=-u_{z,l}(r) \end{aligned} \tag{19}$$

where $u_{r,l}(r)$, $u_{z,l}(r)$ are the velocities of the droplet surface in the r and z directions, respectively; F_s and F_l are defined by

$$\begin{aligned} F_s&=\lambda_s\frac{2-\sigma_{v,s}}{\sigma_{v,s}}\\ F_l&=\lambda_l\frac{2-\sigma_{v,l}}{\sigma_{v,l}} \end{aligned} \tag{20}$$

where λ_s and λ_l are the mean free paths of the gas molecules near the solid and the droplet surfaces, respectively.

Eqs. (16) and (17) can be solved by using a similar procedure as given by Ge and Fan [24]. Thus the vapor pressure can be determined by

$$p(r)=p_0+\int_r^{R_0}\rho\varphi(r)\,dr \tag{21}$$

where R_0 is the radius of the extent of the vapor layer and $\varphi(r)$ is given by

$$\varphi(r)=\frac{2vC_1}{\delta^2}\bar{u}_r-\frac{\bar{u}_r u_{zl}}{\delta}(B_1-B_2)+\frac{\bar{u}_r^2}{r}B_1 \tag{22}$$

where

$$\begin{aligned} B_1&=\frac{C_1^2}{5}+\frac{C_1C_2}{2}+\frac{2C_1C_3+C_2^2}{3}+C_1C_3+C_3^2\\ B_2&=\frac{2C_1^2}{15}+\frac{C_1C_2}{3}+\frac{C_2^2}{6}+\frac{2}{3}C_1C_3+\frac{1}{2}C_2C_3\\ C_1&=-3\frac{2+2k_l+2k_s-\theta_l-2k_s\theta_l}{1+k_l+4k_s+6k_lk_s}\\ C_2&=\frac{6+6k_l-2\theta_l}{1+k_l+4k_s+6k_lk_s}\\ C_3&=k_sC_2 \end{aligned} \tag{23}$$

where $k_l=\frac{F_l}{\delta}$, $k_s=\frac{F_s}{\delta}$, $\theta_l=\frac{u_{r,l}}{\bar{u}_r}$. The averaged velocity of the vapor can be expressed by

$$\bar{u}_r(r)=\frac{1}{r\delta(r)}\int_0^r r'u_{z,l}(r')\,dr' \tag{24}$$

The pressure distribution in the vapor layer can be obtained by solving Eqs. (21)–(24) by a piecewise integration method. In this procedure, the thickness of the vapor layer $\delta(r)$ is obtained from the level-set function at the cells in the vicinity of the solid surface. The local evaporation rate, $\dot{m}=\rho u_{z,l}(r)$, is defined by the heat transfer model, i.e. Eq. (15). The vapor pressure force simulated by this model is applied as an interface force to the droplet bottom surface.

3. Results and discussion

Three different subcooled impact conditions under which the experiments were conducted and reported in the literature are simulated in this study. They are (1) *n*-heptane droplets (1.5 mm diameter) impacting on the stainless steel surface with $We=43$ [6], (2) 3.8 mm water droplets impacting on the inconel surface at a velocity of 1 m/s [12], and (3) 4.0 mm water droplets impacting on the copper surface with $We=25$ [5]. The simulation is conducted on uniform Cartesian meshes ($\Delta x=\Delta y=\Delta z=\Delta$). The mesh size (resolution) is determined by considering the mesh refinement criterion, in which finer meshes yield negligible difference in computation results when the CPR (cells per droplet radius) is larger than 12–15 [24]. Thus, the mesh sizes in this study are chosen to provide a resolution of CPR = 15. The time steps (Δt) are determined by considering various conditions including the CFL (Courant–Friedrichs–Levy) condition and the constraints of viscous and surface tension [32]. With $100\times100\times100$ grid points, it takes 20–24 h for the Cray-94 supercomputer at the Ohio Supercomputer Center (OSC) to complete a typical droplet impact case in real time of 20–40 ms.

Fig. 2 shows the comparison of the photographs from Chandra and Avedisian [6] with simulated images of this study for a subcooled 1.5 mm *n*-heptane droplet impact onto a stainless-steel surface of 200 °C. The impact velocity is 93 cm/s, which gives a Weber number of 43 and a Reynolds number of 2300. The initial temperature of the droplet is the room temperature (20 °C). The photographs were taken by using single-shot flash photography, which assumes the droplet impact process is repeatable from one experiment to another [6]. The mesh resolution of the simulation is 0.05 mm in grid size. In Fig. 2, each image is compared with the photograph of the droplet taken at same instance in time (t) after the impact. It can be seen that the evolution of droplet shapes are well simulated by the computation. In the first 2.5 ms of the impact (frame 1 to frame 2), the droplet spread out right after the impact, and a disk-like shape liquid film is formed on the surface. The behavior is caused by the inertial force, which drives the liquid to spread on the solid surface, while the surface tension and the viscous forces at the edge of the droplet resist the spreading of the liquid film. The speed of the

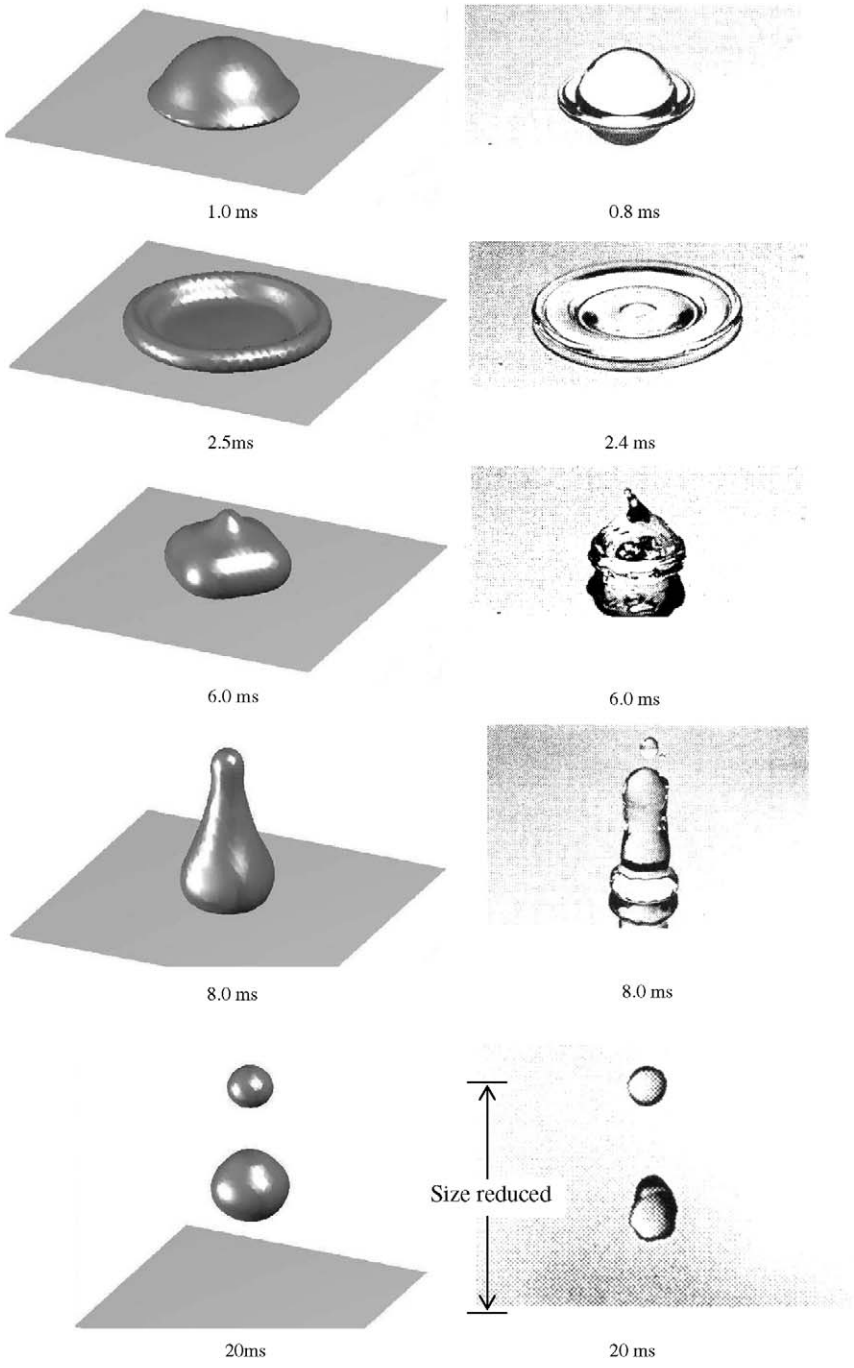

Fig. 2. *n*-Heptane droplet collision with the surface at 200 °C. Experimental images (right) are presented by Chandra and Avedisian [6]. $We = 45$. The size of the last frame is reduced.

outward moving front of the droplet gradually decreases and the fluid starts to accumulate at the leading edge of the liquid film (2.5 ms). When the droplet reaches the maximum diameter at about 2.1 ms, the surface energy also reaches to its maximum. Then, the liquid film starts to retreat back to its center (frames 2 and 3) due to the surface tension force induced from the periphery of the droplet. Beyond 6.0 ms, the droplet continues to recoil and forms an upward flow in the center of the droplet (frames 3 and 4), which leads to the bouncing of the droplet up from the surface (frame 5). The photograph at 8.0 ms shows that the tip of the elongated droplet separates from the main body of the droplet and the main body of the droplet then breaks up into smaller secondary drops (frame 5). This phenomenon was reproduced accurately in the simulation (frame 5). Note that the scale of the last frame (20 ms) in Fig. 2 is reduced to cover a larger range in the z-direction.

Fig. 3 shows the detailed spreading process of the droplet during the same impact shown in Fig. 2 from a viewing angle of 60° instead of 20° in Fig. 2. Experimental images show that a hole is formed in the center of the droplet for a short time period (3.4–4.8 ms) and the center of the

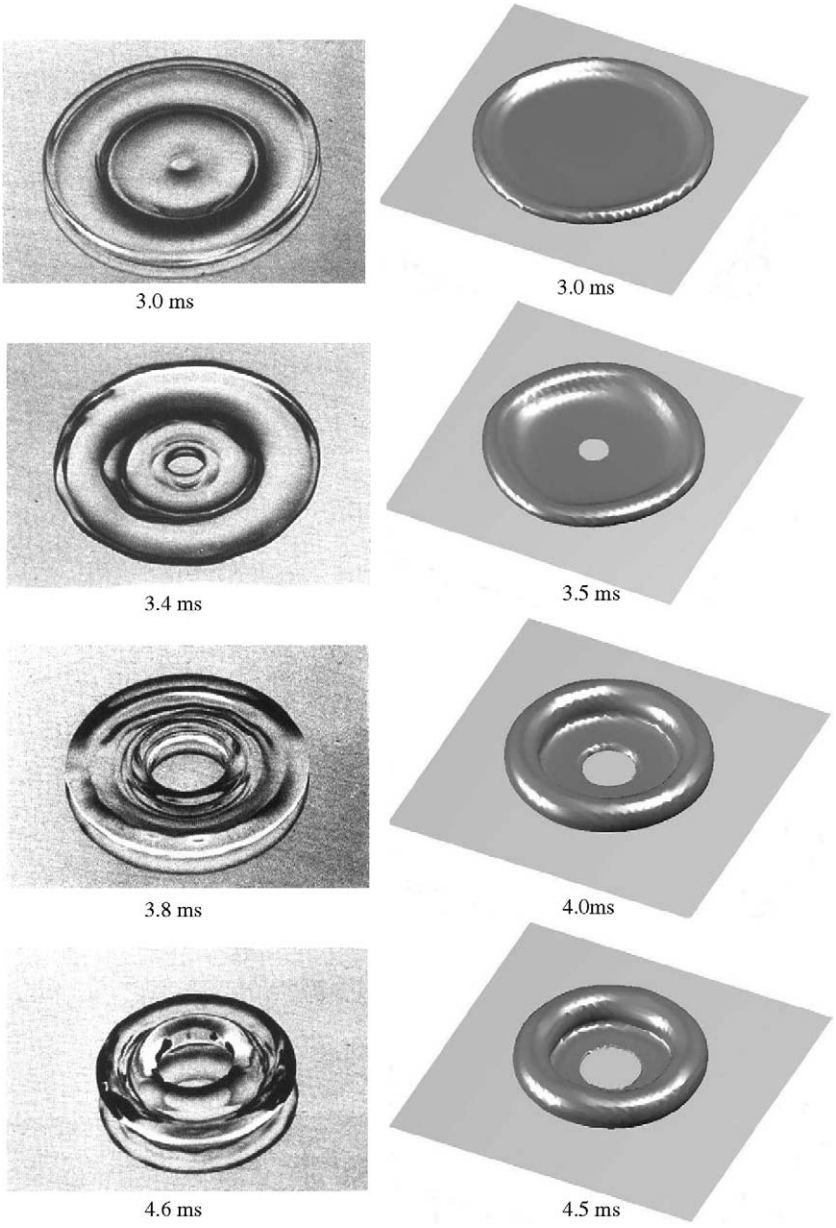

Fig. 3. Experimental photos (left) by Chandra and Avedisian [6] and simulated images (right) of the spreading droplet on the surface at 200 °C. The formation of a hole in the center of the liquid is captured.

liquid droplet is a dry circular area. The simulation also shows this hole structure, although a minor variation exists over the experimental images. As the temperature of the surface is above the Leidenfrost temperature of the liquid, the vapor layer formed between the liquid droplet and the solid surface diminishes the droplet-solid contact, yielding a low surface friction effect on the outward flow of the spreading liquid. When the droplet periphery starts to retreat due to the surface tension effect, the liquid in the droplet center still flows outward driven by the inertial momentum, leading to the formation of the hole structure.

Fig. 4 shows the simulated spread factor of the droplet during the impact shown in Figs. 2 and 3 compared with the measured values of Chandra and Avedisian [6]. The dimensionless height of the center of gravity of the droplet is also plotted in Fig. 4. The spread factor is defined as the radius of the area covered by the deformed droplet on the solid surface divided by the initial radius of the droplet [16]. The spread factor curve reaches a peak at 2.1–2.5 ms after the impact, which corresponds to the maximum extent of the droplet spreading on the surface. In the mean time, the height of the center of gravity of the droplet reaches its minimum. The total residence time of the droplet on the solid surface, which is about 11 ms in this case, can also be determined by the spread factor curve.

The simulated temperature drop of the surface during the droplet impact is shown in Fig. 5. Four curves represent the temperatures at locations with different depths beneath

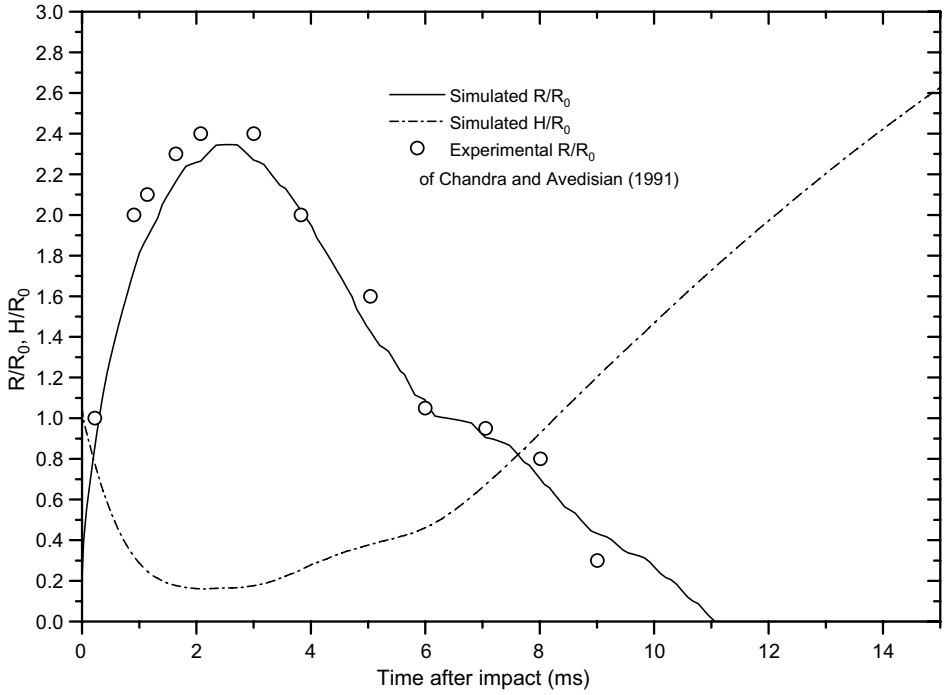

Fig. 4. Spread factor and height of the center of gravity of the droplets versus time for the impact given in Fig. 2.

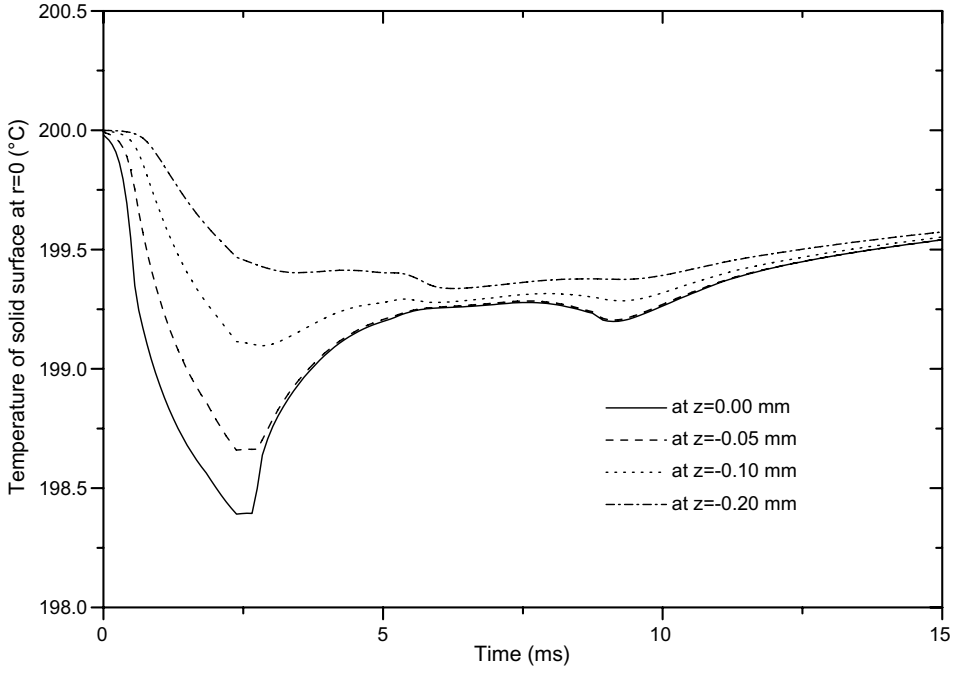

Fig. 5. Solid surface temperature at $r = 0$ at different depths during the impact given in Fig. 2.

the impact point at the surface. Z is the vertical coordinate. Fig. 5 shows that an abrupt temperature drop occurs right after the impingement of the droplet. Then, the temperature recovery starts at 2.7 ms, which is also the transition time of droplet movement from the spreading to the recoiling. The temperature drop of the surface during the impact is around 1–2 °C, which is close to the surface temperature drop estimated by Chandra and Avedisian [6] based on the temperatures measured inside the surface.

The impact process of a 3.8 mm water droplet under the conditions experimentally studied by Chen and Hsu [12] is simulated and the simulation results are shown in Fig. 6. Their experiments involve water droplet impacts on a heated Inconel plate with Nickel coating. The surface

temperature in this simulation is set as 400 °C with the initial temperature of the droplet given as 20 °C. The impact velocity is 1 m/s, which gives a Weber number of 60. In the experiments of Chen and Hsu [12], the temperature history of the surface was measured using a fast-response microthermocouple, while there was no photographing performed on the droplet shapes in the collision process. The simulation is run on a $150 \times 150 \times 100$ mesh, which gives a resolution of 0.01 mm for the grid size (CPR = 20). The first 3 frames of the images show a similar spreading process of the liquid film on the surface as shown in Fig. 2. At 7.0 ms after the impact, the liquid film expands to its maximum, and after that the recoiling occurs which is captured in frames 4 and 5. The hydrodynamic feature of the rebounding is similar to the impact shown in Fig. 2, with an exception that the water droplet still maintains

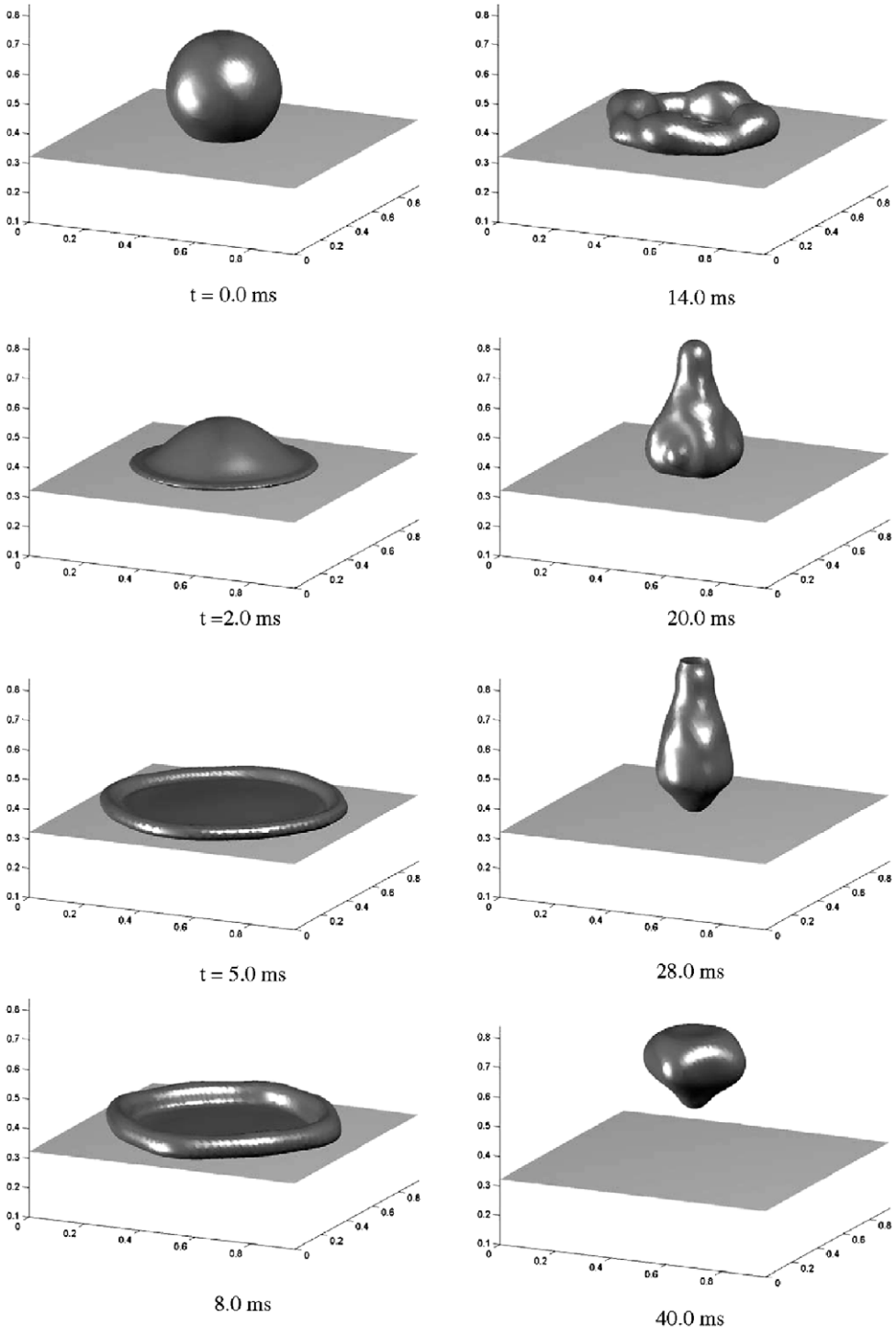

Fig. 6. Water droplet impacts on a flat surface with $We = 60$. The initial droplet diameter is 3.8 mm and surface temperature is 400 °C.

itself as an integrated mass. It is also noted that in this case, with a larger droplet size (3.8 mm) and higher impact Reynolds number compared with the case in Fig. 2, the droplet undergoes wider spreading, which yields a longer residence time on the surface.

In Fig. 6, a square droplet contact area with the solid surface is seen at the end of the spreading stage ($t = 8.0$ ms), which is followed by an asymmetrical recoiling droplet shape at 14.0 ms (frame 5). The occurrence of the square shape, which was also addressed by Bussmann et al. [16] in the 3-D simulation of droplet impact on an isothermal surface, is mainly caused by the use of the uniform Cartesian mesh. The mesh refinement study conducted by Ge and Fan [24] has shown that using a finer mesh can refine the droplet contact shape. Even though the asymmetry of the droplet structure variation is shown in Figs. 2 and 6, the overall droplet dynamics, quantified by the contact time, the spreading factor and the droplet height, can still be accurately reproduced with the current mesh resolution.

The spreading factors and the height of the center of gravity of the droplet for the impact condition shown in Fig. 6 are given in Fig. 7. It can be seen that the residence time of the droplet on the surface is about 30 ms, which is close to the experimental results of Chen and Hsu [12]. It is noted that the first order vibration period of the oscillating drop is considered to be equal to the residence time of the droplet [24]. It can also be found that at around 7–8 ms after the impact, the deformed droplet reaches the maximum radius on the solid surface, which is nearly twice the initial radius of the droplet. Thus 7–8 ms can be considered as the transition time of the droplet from the spreading process to recoiling process.

Fig. 8 shows the calculated temperature distributions within the droplet and the solid surface. The isotherm corresponding to 21 °C is plotted inside the droplet to represent the extent of the thermal boundary layer of the droplet that is affected by the heating of the solid surface. It can be seen that, in the droplet spreading process (0–7.0 ms), the bulk of the liquid droplet remains at its initial temperature and the thermal boundary layer is very thin. As the liquid film spreads on the solid surface, the heat transfer rate on the liquid side of the droplet–vapor interface can be evaluated by

$$q_{\text{drop}} = k_{\text{l}} \frac{T_{\text{d2}} - T_{\text{d,bulk}}}{\delta_{\text{T}}} \tag{25}$$

where δ_{T} is the thickness of the thermal boundary layer; T_{d2} and $T_{\text{d,bulk}}$ are the droplet temperature at the surface and in the bulk, respectively. The thermal boundary layer thickness can be estimated by [33]:

$$\delta_{\text{T}} = \frac{2d_0}{Re^{0.5}Pr^{0.4}} \tag{26}$$

where Re is the Reynolds number of the spreading liquid flow and is defined by $Re = \frac{\rho V d_0}{\mu}$; and V is the liquid film velocity. At the early stage of the spreading, V is close to the initial impact velocity of the droplet, and thus, it gives a thin thermal boundary layer as shown in frames 1 and 2 of Fig. 8. When the droplet spreads to the maximum extent and starts to recoil, the liquid velocity diminishes to zero and the thermal boundary layer is disrupted. Until then,

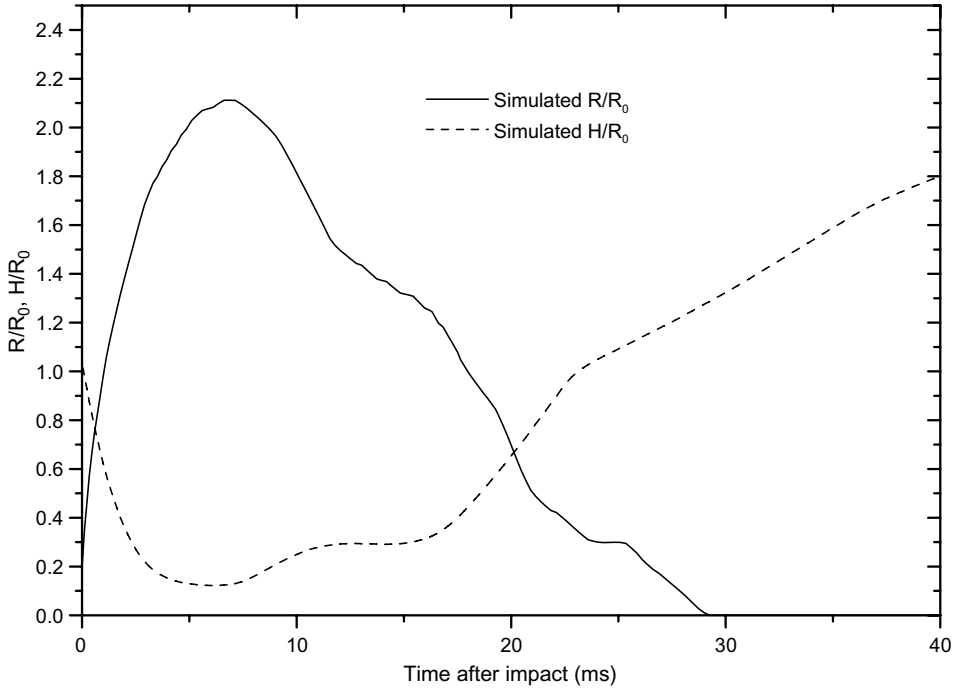

Fig. 7. Spread factor and height of the center of gravity of the droplets during the impact given in Fig. 6.

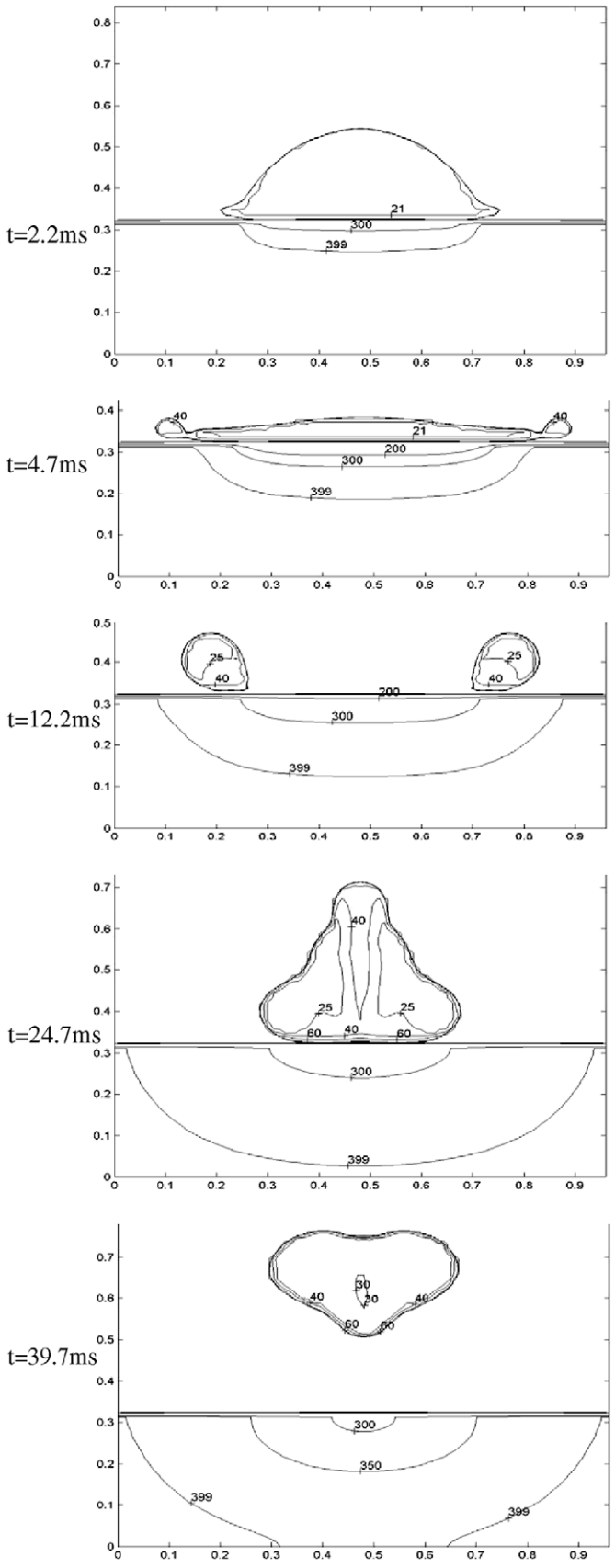

Fig. 8. Simulated temperature field in the liquid and the solid phases for the impact given in Fig. 6.

the temperature rise inside the droplet becomes significant (frames 3 and 4 of Fig. 8). After the droplet rebounds from the solid surface (frame 5), the overall temperature increase for the droplet during the impact is about 15–20 °C. The simulated temperature distribution inside the solid surface is also shown in Fig. 8, in which the isotherm of 399 °C is chosen to represent the area of temperature drop during the impact of the droplet.

The surface temperature history at the center of the impact ($r = 0$) is shown in Fig. 9, and the prediction results for different depths are compared with the measurements given by Chen and Hsu [12]. A dramatic temperature drop (>250 °C) occurs during the first 0–7 ms of the impact, which, as shown by Figs. 6 and 7, reflects the spreading process. After that, the surface temperature recovers in the recoiling stage implying a lower heat transfer rate at the surface. The simulated surface temperature agrees well with the measurements before 10 ms. After that, the simulation predicts a slower recovery process compared with the experiments. This discrepancy is caused by the difference between the real experimental conditions and the idealized simulation condition, which will be elaborated later. Compared with the surface temperature drop during the impact of the *n*-heptane droplet shown in Fig. 5, the impingement of the water droplet yields a much larger temperature drop on the surface, and also a higher heat flux.

The transient heat flux at the center of the impact of the solid surface is shown in Fig. 10. The results of Chen and Hsu [12] shown in this figure are calculated based on the measured surface temperature through a one-dimension model. The simulated heat flux rapidly reaches a peak at 0.5–1.0 ms and then drops and oscillates at a level of about 1000–1500 W/cm^2. This rapid drop in the heat flux can be explained by examining the surface temperature curves in Fig. 9. Since the heat conductivity of the Inconel is relatively low, the contact of the droplet and solid surface at the beginning of the impact causes a significant temperature drop (~250 °C) of the solid surface (shown in Fig. 9). Because of the slow heat transfer rate inside the solid, the heat flux at the surface cannot be sustained and rapidly drops to 1000 W/cm^2. After 7–8 ms, the heat flux at $r = 0$ falls to around zero for both the present simulation and the experiment-based calculation. This behavior can be explained by the increasing thickness of the vapor layer in the recoiling process, which hinders the heat transfer between the surface and the droplet.

Fig. 11 shows the calculated surface heat flux distribution in the radial direction. It is seen that the highest heat flux (>3000 W/cm^2) is achieved right after the droplet impact (0.6 ms). As the droplet spreads further, the heat transfer area increases and the averaged heat flux decreases. The distribution of the heat flux is relatively uniform except in the area near the periphery of the droplet, where the heat flux reaches its maximum (1.3–5.5 ms). This is due to the fact that at this area the surface temperature is

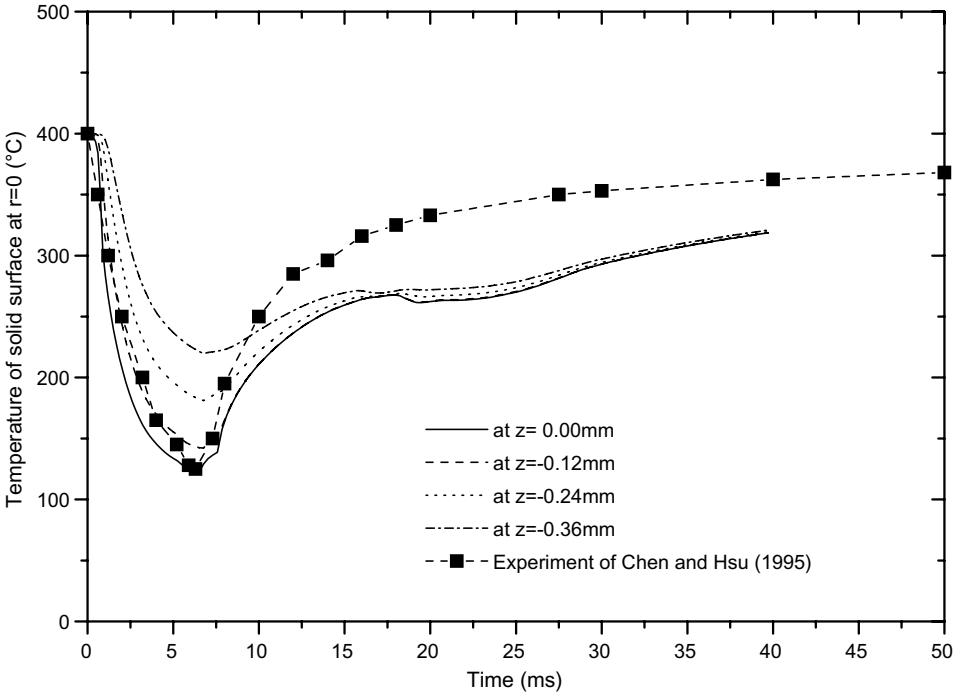

Fig. 9. Simulated solid surface temperature at $R = 0$ at different depths compared with the experimental results reported by Chen and Hsu [12].

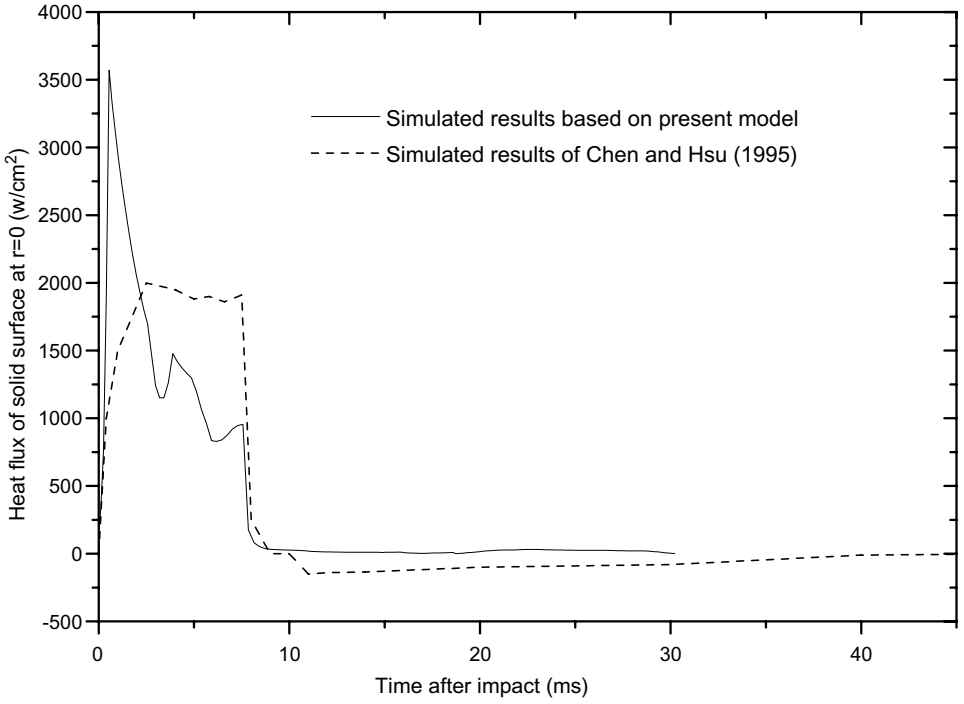

Fig. 10. The simulated results on the heat flux based on the present model in comparison with those based on the one-dimensional model reported by Chen and Hsu [12].

still maintained at a higher level compared with the center portion of the contact area. Again, the heat flux is found to be relatively small after the spreading (0–8 ms).

Fig. 12 shows the simulated total heat flux of the solid surface during the impact. It can be seen that the major portion of the heat loss of the surface occurs during the droplet spreading process (0–8 ms). The inverse effects of the contact area and the surface temperature on the total heat transfer rate yield the U-shaped curve during this period. It can be concluded that the heat loss on the solid

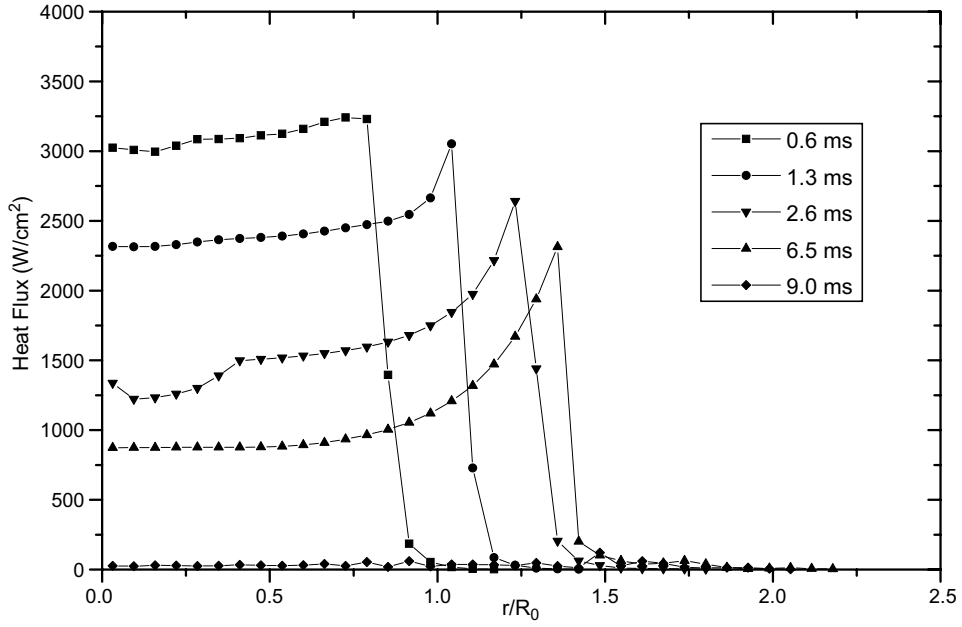

Fig. 11. Simulated heat flux distribution in the radial direction.

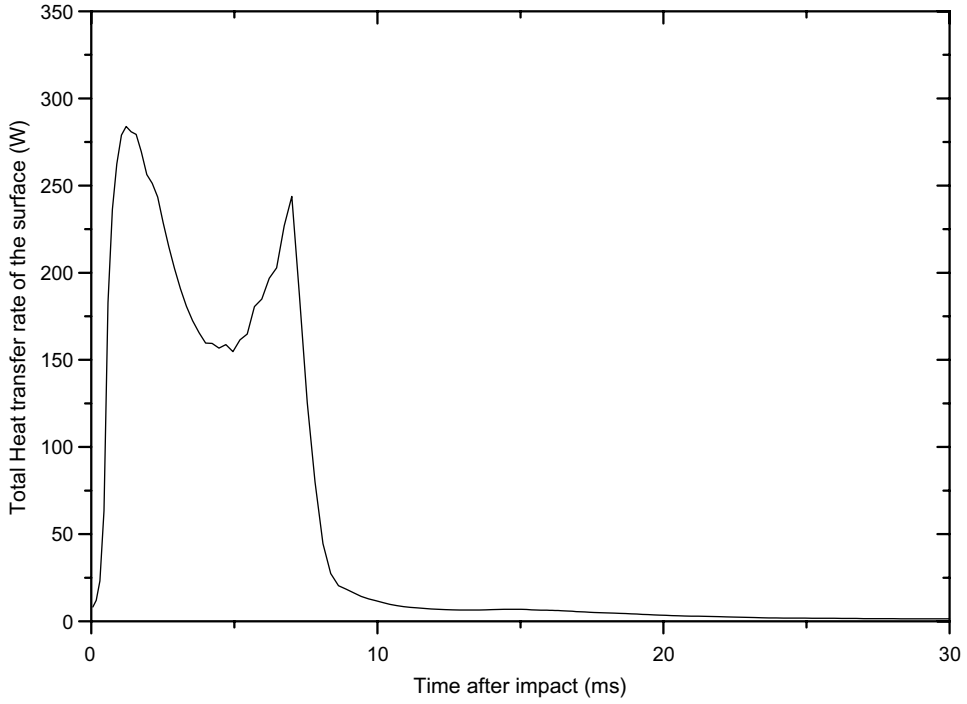

Fig. 12. Simulated total heat flux at the solid surface.

surface occurs mainly during the spreading process of the droplet.

As mentioned earlier, the simulation of the droplet impact can be conducted under perfectly symmetrical conditions with respect to the droplet velocity relative to the solid surface. This condition is however not easy to achieve in the experiments. As the droplet is released from the nozzle and moves toward the superheated surface, some uncontrollable factors such as the angle of dropping, which corresponds to the dropping condition with non-negligible tangential velocity, obliquity of the surface and perturbation of the ambient condition render it difficult to maintain a perfectly normal collision between the droplet and solid surface such that the collision takes place at one fixed location throughout the entire impact process. The 3-D simulation of this study is capable of reproducing the imperfect droplet–surface impact condition represented by unsymmetrical collision. Fig. 13 shows the simulated 3-D images

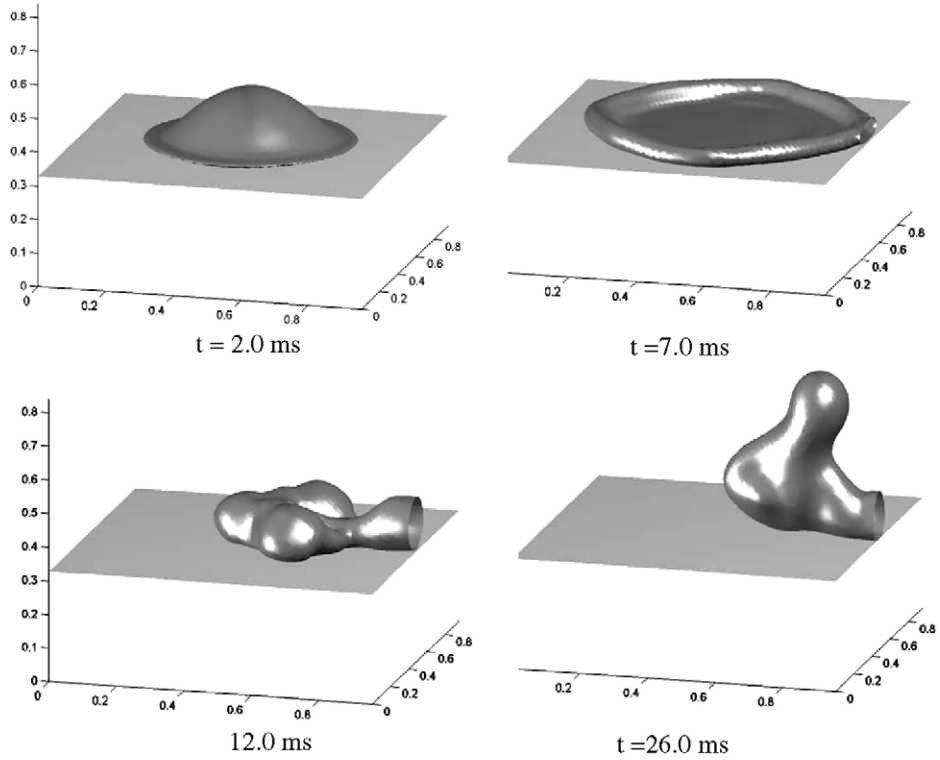

Fig. 13. Droplet impacts on a flat surface with a small tangential velocity. Other impact conditions are the same as those given in Fig. 6.

of the droplet under the same impact condition as that shown in Fig. 6 but with a 5 cm/s tangential velocity. The simulated temperature is shown in Fig. 14 with comparisons with the experimental measurements of Chen and Hsu [12]. It can be seen that with a small obliquity, there is a significant effect on the movement behavior of the droplet. Specifically, in this case, the droplet moves away from the impact center during the recoiling process

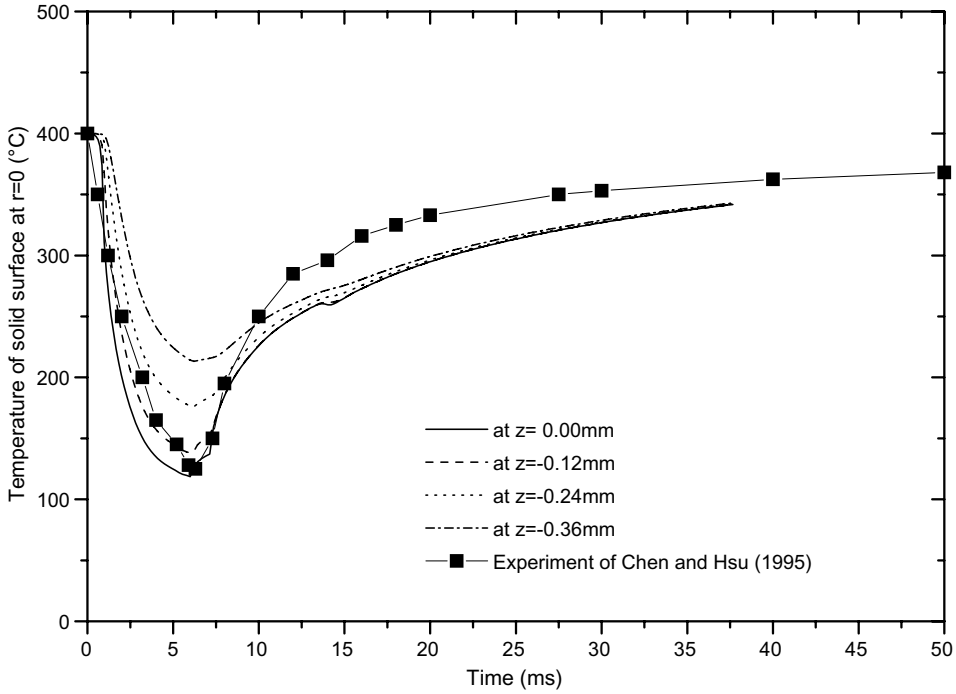

Fig. 14. Simulated solid surface temperatures in comparison with the experimental results of Chen and Hsu [12]. The impact has a small tangential velocity (5 cm/s) as given in Fig. 13.

leading to a faster recovery of the solid surface temperature (shown in Fig. 14).

Further simulations were conducted for the experimental conditions of Inada et al. [5]. In their experiments, a 4.0 mm water droplet impacts on a heated platinum surface at a temperature up to 420 °C. The subcooling degree of the droplet (δT_{sub}) varied from 2 °C to 88 °C. The droplet falls from a location which is 20 mm above the surface with an impact velocity which can be estimated as 64 cm/s corresponding to a Weber number of about 25. In this simulation, the initial temperature of the surface is fixed at 420 °C, which ensures the non-wetting contact between the droplet and the surface. The simulated droplet dynamics are similar to the impact shown in Fig. 6, except for a longer spreading process. The surface temperature changes in the impact with ($\delta T_{sub} = 88$ °C) are shown in Fig. 15.

In order to estimate the heat flux at the surface in the experiment, Inada et al. [5] welded four thermocouples at different locations underneath the impact point inside the solid surface. Fig. 15 shows the simulated solid temperature compared with the measured value at two locations. T_1 and T_2 correspond to the temperatures measured at 0.28 mm and 0.74 mm, respectively, beneath the surface. It is seen that the simulated surface temperatures agree well with the measured T_1 and T_2; both decrease with time after the impact until 13–14 ms when they increase. The simulated temperature at the surface of the solid (T_w) is also shown in Fig. 15. The maximum temperature drop at the surface is ~60 °C, which occurs about 13 ms after the impact. Compared with the temperature drop (250 °C) in Fig. 9, it can be seen that the temperature drop in this case is relatively small. The reason for this difference is that the heat conductivity of copper in this case is much higher than that of Inconel used in the experiments for the results shown in Fig. 9.

The current simulation model is applied to analyze the effects of the initial temperature of the droplet. With the remaining conditions unchanged and consistent with the experiment of Inada et al. [5], the simulation is conducted for three different subcooling degrees: $\delta T_{sub} = 2$ °C, 30 °C and 88 °C. The results are shown in Figs. 16–18.

Fig. 16 shows the simulated solid surface temperature at the center of the impact. It can be seen that the droplet subcooling has a significant effect on the temperature drop of the surface. For a droplet near the saturated condition ($\delta T_{sub} = 2$ °C), the surface temperature drop is about 8–10 °C. However, with a high degree of subcooling ($\delta T_{sub} = 88$ °C), the surface temperature drop reaches 60 °C. The effect of the droplet subcooling is also reflected on the heat flux at the solid surface in Fig. 17. The averaged heat flux shown in Fig. 17 is calculated based on the total heat flux (Q_w) on the surface and the contact area:

$$\bar{q}_w = \frac{Q_w}{\pi R_0^2} \tag{27}$$

For the impact with a high degree of subcooling ($\delta T_{sub} =$ 88 °C), the average heat flux at the solid surface is 1500–1800 W/cm^2 during the droplet spread and gradually reduces to 100–200 W/cm^2 in the recoiling stage. The averaged heat flux for impact with a less subcooled droplet is much lower. For the droplet impact with $\delta T_{sub} = 2$ °C, the heat flux at the surface during the droplet spread is only 200–300 W/cm^2, which is an order of magnitude less than that for $\delta T_{sub} = 88$ °C. In the boiling curve of the droplet

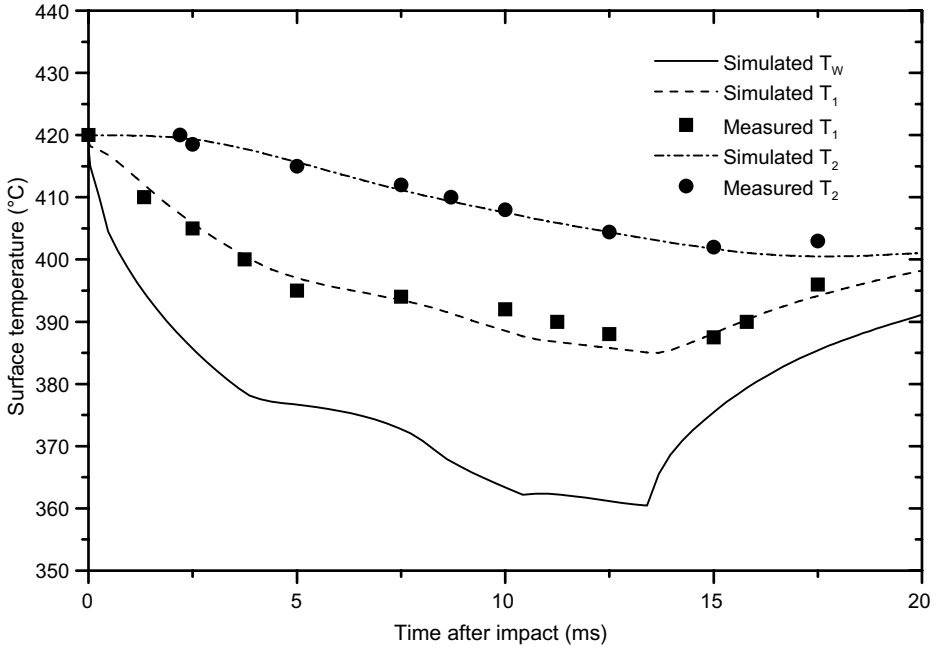

Fig. 15. Simulated solid surface temperatures in comparison with the experimental results of Inada et al. [5]. T_1 and T_2 are the temperatures at locations inside the surface with $z_1 = 0.28$ mm and $z_2 = 0.74$ mm, respectively.

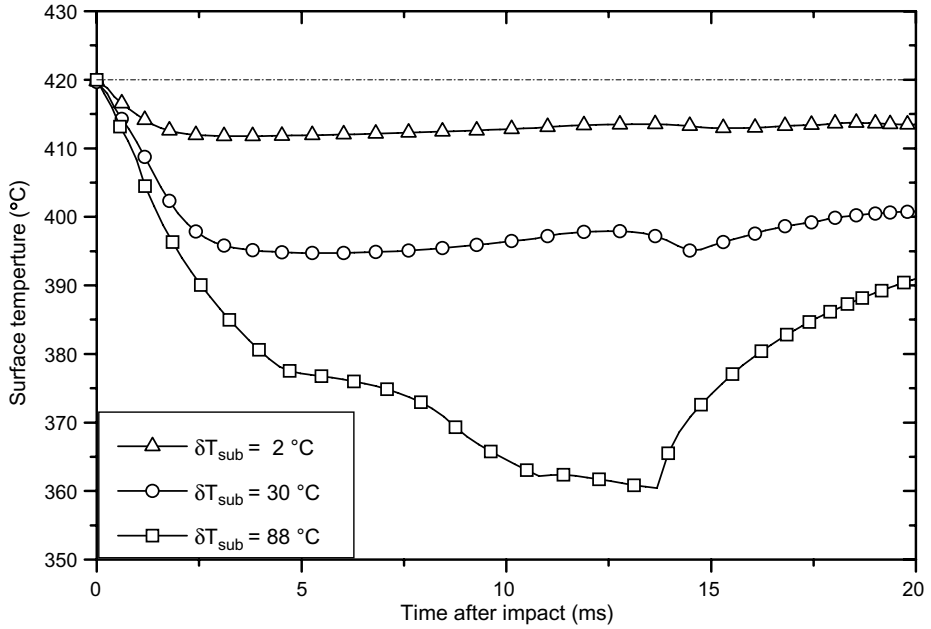

Fig. 16. The effect of the subcooling degree of the droplet on the transient temperature variation of the heated surface.

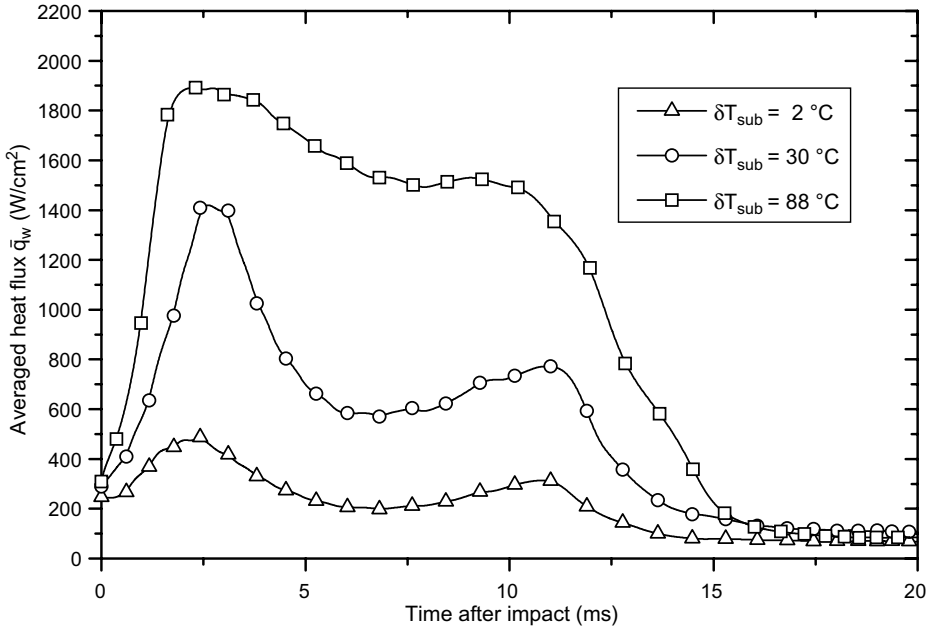

Fig. 17. Averaged heat flux across the contact area during the impacts at different subcooling degrees of the droplet.

[5], the time averaged heat fluxes were given based on the measurements. For the initial surface temperature of 420 °C, the averaged heat flux was reported to be 1.5×10^7, 0.8×10^7 and 0.2×10^7 W/m^2 for droplet impacts with respect to subcooling degrees, δT_{sub}, of 88 °C, 30 °C and 2 °C, respectively. Compared with their results, the present model exhibits high accuracy in the prediction of the effect of the droplet subcooling.

To understand the effects of the droplet subcooling degree on the surface temperature and heat flux, the averaged thickness of the vapor layer is calculated and shown in Fig. 18. It can be seen that after the initial approach of the droplet surface and the solid surface (0–2 ms), the vapor layer gradually increases from 3 μm to 35 μm when the subcooling degree is small, i.e. $\delta T_{sub} = 2$ °C. For a droplet with a high subcooling degree, δT_{sub}, of 88 °C, the vapor layer thickness is around 0.5–1.0 μm until the recoil (13 ms) occurs. This difference can be explained by considering the energy balance at the liquid–vapor interface (Eq. (15)), where the thermal energy transferred from the solid surface across the vapor layer is balanced by the evaporation latent heat and the heat flux used to heat up

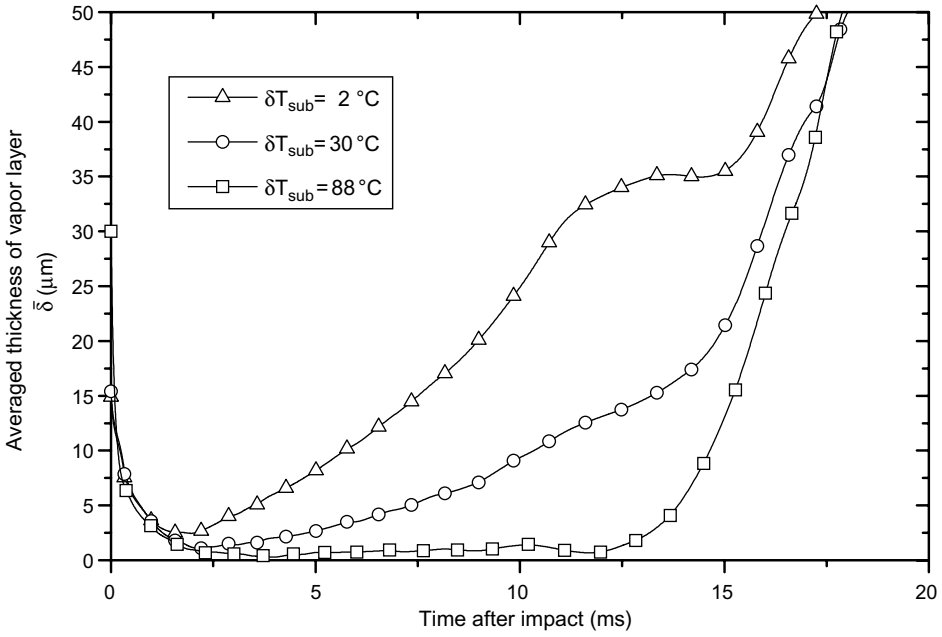

Fig. 18. Variations of the averaged thickness of the vapor layer with time at different subcooling degrees of the droplet.

the bulk liquid (q_l). For a highly subcooled droplet ($\delta T_{sub} = 88$ °C), the heat flux q_l at the droplet surface is large due to the large temperature gradient on the liquid side, which yields a lower local evaporation rate and a lower vapor pressure. Thus, the vapor layer thickness for a highly subcooled droplet is smaller compared with that for a low subcooled droplet. As the vapor layer hinders the heat transfer rate, the impact of a lower subcooled droplet ($\delta T_{sub} = 2$ °C) yields a thicker vapor layer and a lower heat flux on the solid surface.

4. Conclusions

A 3-D model is developed to study the fundamental nature of the heat transfer phenomenon of a subcooled droplet upon impact with a superheated flat surface. The numerical technique adopted in this model involves a Eulerian, fixed-grid and finite-volume algorithm coupled with the level-set methods that tracks the deformation of the droplet surface. The heat transfer properties in each phase are solved with a micro-scale vapor flow model applied to determine the vapor pressure force during the contact process between the droplet and the superheated surface. The model is applied to simulate the impact phenomenon of water and *n*-heptane on a heated surface with different properties. The simulation results are compared with the experimental measurements of the droplet deformation process and the surface temperature variation reported in the literature. The comparison shows a good agreement.

The impact of the *n*-heptane droplet induces a much lower temperature drop at the solid surface compared with that of the water droplet. The decrease in the solid surface temperature occurs mainly during the droplet-spreading stage, and it recovers at the recoiling stage due to the presence of the fully established vapor layer. On the other hand, the bulk of the liquid droplet remains at its initial temperature in the droplet-spreading process with a thin thermal boundary layer present in the surface. The temperature rise inside the droplet becomes significant, however, only in the droplet recoiling process. During the droplet spreading, the distribution of the heat flux is relatively uniform through the droplet–solid surface contact area except near the periphery of the droplet. During the droplet recoiling, the heat flux is relatively small. The analysis of the effects of the droplet initial temperature indicates that the droplet subcooling degree is closely related to the thickness of vapor layer and the heat flux at the surface. As the subcooling degree of the a water droplet increases from 2 °C to 88 °C, the heat flux at the surface during the droplet impact increases by as much as one order of magnitude.

Acknowledgements

We appreciate the insightful comments by Professor John Chen of Lehigh University in the formulation of this problem. The support of the Ohio Supercomputer Center on the computation work conducted in this study is gratefully acknowledged.

References

[1] M. Rein, Phenomena of liquid drop impact on solid and liquid surfaces, Fluid Dyn. Res. 12 (1993) 61–93.
[2] L.-S. Fan, R. Lau, C. Zhu, K. Vuong, W. Warsito, X. Wang, G. Liu, Evaporative liquid jets in gas–liquid–solid flow system, Chem. Eng. Sci. 56 (2001) 5871–5891.
[3] B.S. Gottfried, C.J. Lee, K.J. Bell, The Leidenfrost phenomenon: film boiling of liquid droplets on a flat plate, Int. J. Heat Mass Transfer 9 (1966) 1167–1187.

[4] L.H.J. Wachters, N.A.J. Westerling, The heat transfer from a hot wall to impinging water drops in the spheroidal state, Chem. Eng. Sci. 21 (1966) 1047–1056.
[5] S. Inada, Y. Miyasaka, K. Nishida, Transient heat transfer for a water drop impinging on a heated surface, Bull. JSME 28 (1985) 2675–2681.
[6] S. Chandra, C.T. Avedisian, On the collision of a droplet with a solid surface, Proc. R. Soc. Lond. A 432 (1991) 13–41.
[7] M. Bussmann, J. Mostaghimi, S. Chandra, Modeling the splash of a droplet impacting a solid surface, Phys. Fluids 12 (12) (2000) 3121–3132.
[8] A.-L. Biance, C. Clanet, D. Quere, Leidenfrost drops, Phys. Fluids 15 (6) (2003) 1632–1637.
[9] Y.M. Qiao, S. Chandra, Boiling of droplet on a hot surface in low gravity, Int. J. Heat Mass Transfer 39 (7) (1996) 1379–1393.
[10] N. Hatta, H. Fujimoto, K. Kinoshita, H. Takuda, Experimental study of deformation mechanism of a water droplet impinging on hot metallic surface above the Leidenfrost temperature, J. Fluids Eng. 119 (1997) 692–699.
[11] S. Inada, W.J. Yang, Film boiling heat transfer for saturated drops impinging on a heating surface, Int. J. Heat Mass Transfer 37 (16) (1994) 2588–2591.
[12] J.C. Chen, K.K. Hsu, Heat transfer during liquid contact on superheated surfaces, J. Heat Transfer 117 (1995) 693–697.
[13] F.H. Harlow, J.P. Shannon, The splash of a liquid droplet, J. Appl. Phys. 38 (1967) 3855.
[14] J. Fukai, Y. Shiiba, T. Yamamoto, O. Miyatake, Wetting effects on the spreading of a liquid droplet colliding with a flat surface: experiment and modeling, Phys. Fluids 7 (2) (1995) 236.
[15] M. Pasandideh-Ford, R. Bhola, S. Chandra, J. Mostaghimi, Deposition of tin droplets on a steel plate: simulation and experiments, Int. J. Heat Mass Transfer 41 (1998) 2929–2945.
[16] M. Bussmann, J. Mostaghimi, S. Chandra, On a three-dimensional volume tracking model of droplet impact, Phys. Fluids 11 (6) (1999) 1406–1417.
[17] V. Mehdi-Nejad, J. Mostaghimi, S. Chandra, Air bubble entrapment under an impacting droplet, Phys. Fluids 15 (1) (2003) 173–183.
[18] M. Francois, W. Shyy, Computations of drop dynamics with the immersed boundary method. Part 1: Numerical algorithm and buoyancy-induced effect, Numer. Heat Transfer B 44 (2003) 101–117.
[19] A. Karl, K. Anders, M. Rieber, A. Frohn, Deformation of liquid droplets during collisions with hot walls: experimental and numerical results, Part. Part. Syst. Charact. 13 (1996) 186–191.
[20] H. Fujimoto, N. Hatta, Deformation and rebounding processes of a water droplet impinging on a flat surface above Leidenfrost temperature, J. Fluids Eng. 118 (1996) 142–149.
[21] D.J.E. Harvie, D.F. Fletcher, A hydrodynamic and thermodynamic simulation of droplet impacts on hot surface. Part I: Theoretical model, Int. J. Heat Mass Transfer 44 (2001) 2633–2642.
[22] D.J.E. Harvie, D.F. Fletcher, A hydrodynamic and thermodynamic simulation of droplet impacts on hot surface. Part II: Validation and applications, Int. J. Heat Mass Transfer 44 (2001) 2643–2659.
[23] A.V. Chizhov, K. Takayama, The impact of compressible liquid droplet on hot rigid surface, Int. J. Heat Mass Transfer 47 (2004) 1391–1401.
[24] Y. Ge, L.-S. Fan, Three-dimensional simulation of impingement of a liquid droplet on a flat surface in the Leidenfrost regime, Phys. Fluids 17 (2005) 027104.
[25] J.U. Brackbill, D.B. Kothe, C. Zemach, A continuum method for modeling surface tension, J. Comput. Phys. 100 (1992) 335–354.
[26] B.A. Kashiwa, N.T. Padial, R.M. Rauenzahn, W.B. Vanderheyden, A cell-centered ICE method for multiphase flow simulation, Los Alamos National Laboratory Research Report, LA-UR-93-3922, 1994.
[27] S. Osher, J.A. Sethian, Fronts propagation with curvature-dependent speed: algorithms based on Hamilton–Jacobi formulation, J. Comput. Phys. 79 (1988) 12.
[28] M. Sussman, E. Fatemi, P. Smereka, S. Osher, An improved level set method for incompressible two-phase flows, Comput. Fluids 27 (5–6) (1998) 663–680.
[29] C. Chen, L.-S. Fan, Discrete simulation of gas–liquid bubble column and gas–liquid–solid fluidized bed, AIChE J. 50 (2004) 288–301.
[30] G.A. Bird, Molecular Gas Dynamics, Clarendon Press, Oxford, UK, 1976.
[31] D.J.E. Harvie, D.F. Fletcher, A simple kinetic theory treatment of volatile liquid–gas interfaces, J. Heat Transfer 123 (2001) 486–491.
[32] M. Sussman, P. Smereka, S. Osher, A level set approach for computing solutions to incompressible two-phase flow, J. Comput. Phys. 114 (1994) 146–159.
[33] M. Pasandideh-Ford, S.D. Aziz, S. Chandra, J. Mostaghimi, Cooling effectiveness of a water drop impinging on a hot surface, Int. J. Heat Fluid Flow 22 (2001) 201.